Available online at www.sciencedirect.com
SCIENCE DIRECT®
Journal of Solid State Chemistry 177 (2004) 1157–1164
JOURNAL OF SOLID STATE CHEMISTRY
http://elsevier.com/locate/jssc

Structural changes produced during heating of the fast ion conductor $Li_{0.18}La_{0.61}TiO_3$. A neutron diffraction study

Jesus Sanz,[a,*] Alejandro Varez,[b] Jose A. Alonso,[a] and Maria.T. Fernandez[c]

[a] *Instituto de Ciencia de Materiales, CSIC, Cantoblanco, E-28049 Madrid, Spain*
[b] *Dpt. of Materiales, Universidad Carlos III de Madrid, E-28911, Leganés, Spain*
[c] *Institut Laue-Langevin, F-38045 Grenoble, France*

Received 21 July 2003; received in revised form 13 October 2003; accepted 26 October 2003

Abstract

The doubled perovskite structure ($2a_p$, $2a_p$, $2a_p$) of the fast ionic conductor $Li_{0.18}La_{0.61}TiO_3$ was investigated between 5 and 773 K by powder neutron diffraction. The Rietveld refinement of this orthorhombic (*Cmmm* Space Group) perovskite showed that at low temperature, La and vacancy rich planes alternate along [001] direction, and TiO_6 octahedra were out-of-phase tilted around the *b*-axis. As temperature increased, the octahedral tilting decreased and the structure approaches, at about 773 K, that of the tetragonal phase, a, a_p, $2a_p$ (*P*4/*mmm* Space Group). In the temperature range of the study, the La-vacancy distribution remained unchanged, but LaO_{12} cuboctahedra became more regular. In the tetragonal phase the elimination of this tilting favors the two-dimensional motion of lithium in alternate *ab*-planes of the perovskite.

Keywords: Lanthanum lithium titanate; High temperature neutron diffraction; Perovskite structure; Ionic conductors

1. Introduction

Interest in $Li_{3x}La_{2/3-x}TiO_3$ perovskites ($0<x<0.167$) has increased since the discovery of their high ionic conductivity ($10^{-3}\,\Omega^{-1}\,cm^{-1}$ at $T = 300$ K) [1,2] and their possible application in electrochemical devices. In Li-poor perovskites, the ordering of La-vacancies was produced in alternate *ab*-planes, favoring a two-dimensional Li conductivity [3–5]. In Li-rich samples, this ordering decreased and the Li conductivity was three-dimensional. However, a closer analysis is required to understand Li ion mobility in these perovskites. In particular, octahedra tilting is a predominant feature that introduces distortions in the oxygen square windows that connect contiguous *A*-sites and could seriously affect Li mobility. By means of X-ray diffraction (XRD) experiments, different symmetries have been found, and related to either a single perovskite or a doubled one along one direction [6–11].

Neutron diffraction (ND) experiments carried out in the Li-poor $Li_{0.12}La_{0.63}TiO_3$ sample, showed that the structure adopted by Li-poor perovskites was orthorhombic, with a unit cell ($2a_p$, $2a_p$, $2a_p$) bigger than that (a_p, a_p, $2a_p$) deduced from XRD experiments [12,13]. This difference was due to the difficulties of the XRD technique to locate oxygen atoms with accuracy. In this perovskite, the axes doubling was produced by La-vacancy ordering along the [001] direction and an out-of phase tilting of octahedra along the *b*-axis. In previous works [3,14], a orthorhombic–tetragonal transformation was detected above 573 K in the Li-poor $Li_{0.18}La_{0.61}TiO_3$ perovskite by XRD. In the temperature range of the study, superstructure peaks associated with La-vacancy ordering did not change. This result suggests that cation disordering is not involved in this transformation.

In this paper, structural changes, during the heating from 5 to 773 K, of the Li-poor perovskite $Li_{0.18}La_{0.61}TiO_3$ are studied by ND. Changes in the geometry and/or the disposition of TiO_6 octahedra are examined, and the structural modifications of the oxygen square windows are related to changes on the Li mobility of the perovskite.

*Corresponding author. Fax: +34-913720623.
E-mail address: jsanz@icmm.csic.es (J. Sanz).

0022-4596/$ - see front matter © 2003 Elsevier Inc. All rights reserved.
doi:10.1016/j.jssc.2003.10.036

2. Experimental

The $Li_{0.18}La_{0.61}TiO_3$ sample was prepared by solid-state reaction of a stoichiometric mixture of high purity $LiOH \cdot H_2O$, La_2O_3 and TiO_2 reagents [2,13]. To reduce the absorption cross section in ND experiments, a ^7Li enriched reagent was used. The Li loss during calcinations was reduced using a slowly heating rate (1°/min). In all the treatments, high-density alumina crucibles were used. Pellets of the reacted powder were fired at 1600 K in air for 6 h. From 1600 K, the sample was cooled slowly (1°/min) to room temperature. For highest temperature treatments, a thin foil of Pt was used to avoid the reaction with alumina. Surface of the pellets were analyzed by EDS microanalysis and Al was not detected. Inductively coupled plasma spectroscopy (ICP) using a JY-70 plus spectrometer was used to determine the metal molar ratio. From the chemical analysis the formula $Li_{0.16(2)}La_{0.62(1)}Ti_{0.98(1)}O_3$ was deduced.

ND patterns were collected in the very high-resolution powder diffractometer D2B at ILL-Grenoble. A wavelength of 1.594 Å was selected from a Ge monochromator. The counting time was 4 h, using about 4 g of sample contained in a vanadium can. ND patterns were taken at increasing temperatures in the 5–773 K range. From 5 to 300 K the cryostat sample environment was used, while high temperature experiments were

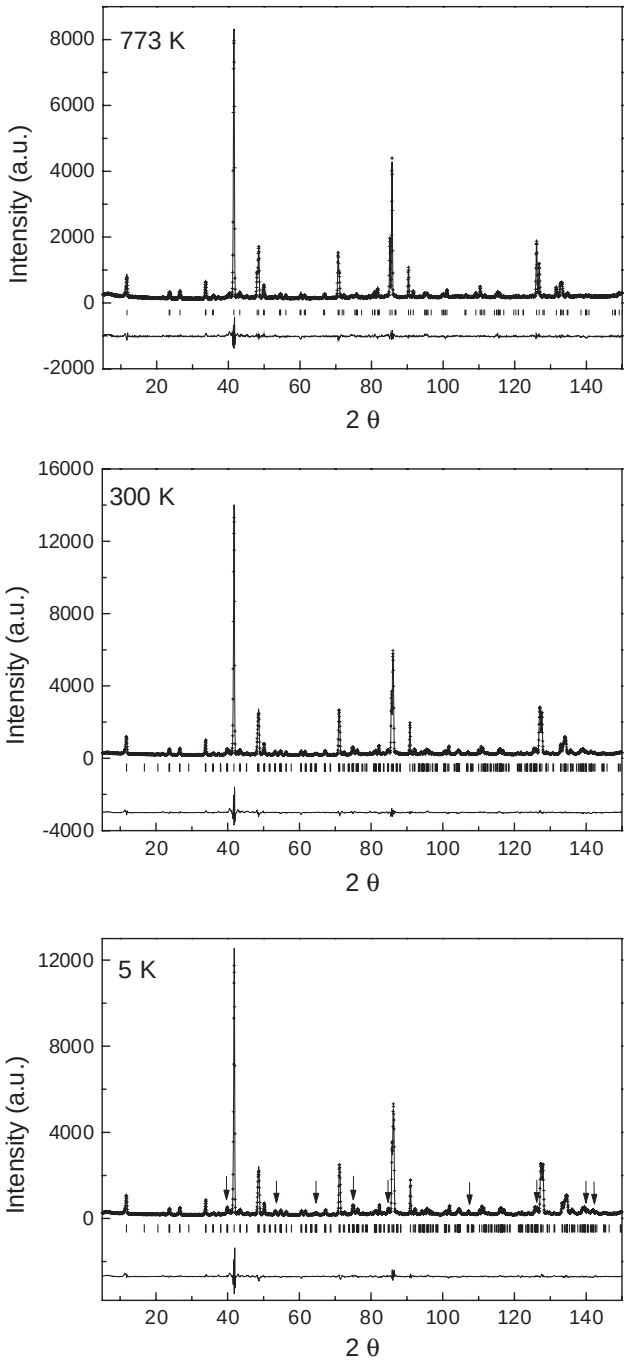

Fig. 1. Refined ND patterns of $Li_{0.18}La_{0.61}TiO_3$ at 5, 300 and 773 K. Peak positions and differences between observed and calculated profiles are included. Arrows denote superstructure peaks of the orthorhombic phase whose intensity progressively decreases with temperature.

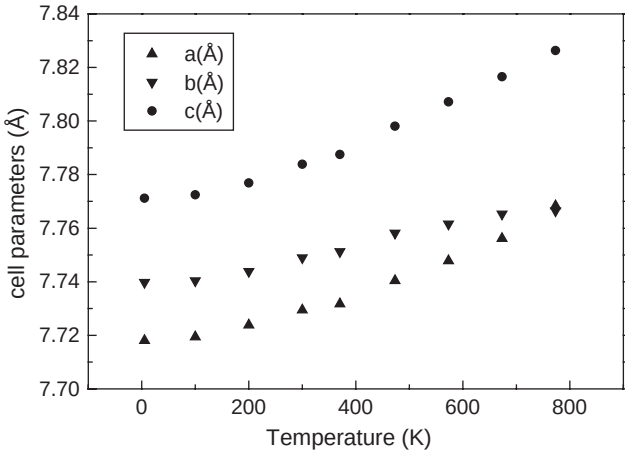

Fig. 2. Lattice parameters of the three-axes doubled $Li_{0.18}La_{0.61}TiO_3$ perovskite as a function of temperature.

Table 1
Structural parameters used in ND pattern refinements with orthorhombic and tetragonal models (Li was not considered)

Atom	Position	S.G. *Cmmm*[a] Atomic coordinates	Atom	Position	S.G *P4/mmm*[b] Atomic coordinates
La1	4*i*	$0, y \approx 1/4, 0$	La1	1*a*	0,0,0
La2	4*j*	$0, y \approx 1/4, 1/2$	La2	1*b*	0,0, $\frac{1}{2}$
Ti	8*o*	$x \approx 1/4, 0, z \approx 1/4$	Ti	2*h*	1/2, 1/2, *z*
O1	4*g*	$x \approx 1/4, 0, 0$	OI	1*c*	1/2, 1/2, 0
O2	4*k*	$0, 0, z \approx 1/4$	OII	4*i*	0, 1/2, *z*
O3	4*l*	$0, 1/2, z \approx 1/4$	OIII	1*d*	1/2, 1/2, 1/2
O4	8*m*	$1/4, 1/4, z \approx 1/4$		—	—
O5	4*h*	$x \approx 1/4, 0, 1/2$		—	—

[a] Taken from Ref. [12].
[b] Taken from Ref. [10].

Table 2
Refined structural parameters for $Li_{0.18}La_{0.61}TiO_3$ between 5 and 773 K using the *Cmmm* Space Group

Atom	Parameter	5 K	100 K	200 K	300 K	370 K	473 K	573 K	673 K	773 K (O)	773 K (T)	Parameter
La1	y/b	0.2555(4)	0.2557(3)	0.2545(6)	0.2546(5)	0.2542(6)	0.2539(6)	0.2532(3)	0.2518(9)	0.2516(11)	—	y/b
	B	0.28(3)	0.38(3)	0.63(4)	0.61(3)	0.82(4)	1.01(4)	1.08(4)	1.30(4)	1.38(4)	1.53(7)	B
	occ	0.966(5)	0.965(6)	0.968(6)	0.969(5)	0.983(6)	0.971(5)	0.959(5)	0.964(5)	0.964(6)	0.97(1)	occ
La2	y/b	0.2621(15)	0.2620(15)	0.2617(21)	0.2616(17)	0.2608(23)	0.2591(23)	0.2583(21)	0.2575(34)	0.256(4)	—	y/b
	B	0.29(14)	0.32(15)	0.66(18)	0.60(15)	0.87(19)	1.11(17)	1.04(15)	1.37(12)	1.40(4)	1.37(26)	B
	occ	0.244(4)	0.238(5)	0.236(5)	0.245(4)	0.235(5)	0.241(5)	0.239(4)	0.241(5)	0.241(5)	0.247(8)	occ
Ti	x/a	0.2477(10)	0.2486(10)	0.2479(12)	0.2477(11)	0.2489(13)	0.2487(13)	0.2489(13)	0.2484(13)	0.249(1)	—	x/a
	z/c	0.2599(4)	0.2596(4)	0.2602(4)	0.2601(4)	0.2606(4)	0.2599(4)	0.2602(4)	0.2603(4)	0.2607(4)	0.2609(7)	z/c
	B	0.37(3)	0.41(3)	0.59(4)	0.55(3)	0.56(4)	0.80(3)	1.02(4)	1.14(4)	1.22(4)	1.25(7)	B
O1	x/a	0.2724(5)	0.2715(5)	0.2712(6)	0.2710(6)	0.2698(7)	0.2678(7)	0.2650(8)	0.2604(10)	0.256(1)	—	x/a (OI)
	B	0.87 (6)	0.91(6)	1.01(7)	1.23(6)	1.03(7)	1.54(7)	1.74(7)	2.13(7)	2.48(8)	2.40(12)	B
O2	z/c	0.2139(4)	0.2137(4)	0.2141(5)	0.2139(4)	0.2136(5)	0.2168(5)	0.2186(6)	0.2207(9)	0.223 (1)	0.2360(4)	z/c (OII)
	B	0.62(6)	0.66(6)	0.91(7)	0.75(6)	0.97(7)	1.11(8)	1.30(8)	1.48(12)	1.59(18)	2.12(5)	B
O3	z/c	0.2612(4)	0.2613(4)	0.2600(5)	0.2592(5)	0.2592(5)	0.2574(5)	0.2569(6)	0.2517(9)	0.245(1)		z/c
	B	0.94(7)	0.89(7)	0.96(8)	1.12(7)	1.21(8)	1.37(9)	1.68(10)	1.82(13)	1.86(23)		B
O4	z/c	0.2329(4)	0.2333(4)	0.2337(4)	0.2341(4)	0.2356(4)	0.2342(5)	0.2346(6)	0.2360(9)	0.238(1)		z/c
	B	1.02(4)	1.03(4)	1.10(5)	1.17(4)	1.11(4)	1.55(5)	1.70(5)	1.87(8)	2.16(11)		B
O5	x/a	0.2314(6)	0.2311(6)	0.2328(7)	0.2304(6)	0.2311(7)	0.2296(7)	0.2303(8)	0.2301(9)	0.235(1)	—	x/a (OIII)
	B	1.06(6)	1.21(6)	1.31(7)	1.27(6)	1.37(7)	1.55(7)	1.95(8)	1.98(9)	2.06(10)	2.71(12)	B
Ti–O1		2.028	2.028	2.033	2.031	2.033	2.032	2.035	2.036	2.040	2.042	Ti–OI
Ti–O2		1.949	1.953	1.951	1.959	1.957	1.954	1.955	1.936	1.943	1.952	Ti–OII
Ti–O3		1.943	1.941	1.945	1.940	1.942	1.945	1.945	1.960	1.960	—	
Ti–O4		1.946	1.946	1.947	1.948	1.947	1.950	1.950	1.950	1.951	—	
Ti–O5		1.871	1.870	1.869	1.874	1.872	1.878	1.878	1.875	1.873	1.871	Ti–OIII
φ (°)		4.7(2)	4.6(2)	4.6(3)	4.6(2)	4.5(3)	4.5(1)	3.9(3)	3.4(4)	2.4(4)	0	
	R_I	6.94	7.23	8.40	6.41	7.25	6.13	5.80	6.10	6.60	5.87	R_I
	R_F	7.73	7.84	8.81	6.75	8.03	7.87	9.24	9.70	9.77	8.71	R_F
	R_P	5.12	5.29	5.69	5.03	5.08	4.89	4.52	4.67	4.90	5.19	R_P
	R_{WP}	7.16	7.38	7.76	7.10	7.29	6.74	6.35	6.72	6.73	7.83	R_{WP}
	R_{exp}	2.67	2.67	2.66	2.57	2.66	3.63	3.16	3.17	3.18	3.20	R_{exp}
	χ^2	7.18	7.62	8.50	7.64	7.53	3.44	4.04	4.49	4.49	5.51	χ^2

At the highest temperature, the tetragonal $P4/mmm$ model has also been tested. Ti–O distances and octahedral tilt angles (φ) are given in Å and degrees, respectively.

carried out in a furnace. A pseudo-Voigt function was chosen to reproduce the line shape of diffraction peaks in structural refinements carried out with the Fullprof program. In this analysis, coherent lengths used for La, Li, Ti and O were 8.24, −1.90, −3.45 and 5.80 fm.

3. Results

The room temperature XRD pattern of the $Li_{0.18}La_{0.61}TiO_3$ sample was indexed with the orthorhombic a_p, a_p, $2a_p$ unit-cell (*Pmmm* Spage Group), where a_p stands for the cell parameter of the ideal cubic perovskite. As reported previously [3,14], a change of symmetry from orthorhombic to tetragonal was detected between 600 and 800 K.

In order to analyze this structural change, ND experiments were carried out as a function of the temperature. In Fig. 1, ND patterns of the sample heated at three different temperatures (5, 300 and 773 K) are shown. Indexing of ND patterns with the unit cell a_p, a_p, $2a_p$ deduced by X-ray was not successful, and left a number of un-indexed peaks (marked with arrows in Fig. 1). As in the case of the Li-poor perovskite, $Li_{0.12}La_{0.62}TiO_3$ [12,13], all the peaks were indexed when the orthorhombic $2a_p$, $2a_p$, $2a_p$ unit cell was considered.

The intensity of the un-indexed peaks decreased as the temperature increased displaying very low intensity at

773 K. From this fact, the high temperature phase was also indexed with the tetragonal a_p, a_p, $2a_p$ unit cell ($P4/mmm$ Space Group). During the heating of the sample, the intensity of the superstructure peaks related to the c-axis doubling (the most characteristic appear at $2\theta \approx 11.7°$) did not change. This coincides with the result obtained with XRD [14].

In Fig. 2 the evolution of the unit cell parameters, deduced from ND patterns, is shown as a function of the temperature. Below 400 K, thermal expansion was isotropic, but above this temperature the expansions of the c- and a-axes are major than that of the b-axis. Differences between a- and b-axes decreased with temperature, and both parameter are basically equal at 773 K. The ND pattern of the sample heated at 773 was indexed with the tetragonal unit cell $a = 3.876$ Å and $c = 7.816$ Å.

To determine the structural changes produced during the orthorhombic–tetragonal transformation a Rietveld analysis of ND patterns collected at increasing temperatures was carried out. In a first step, Li ions were not considered because their small contribution to ND patterns. For the structural analysis of samples heated between 5 and 773 K, the orthorhombic $2a_p$, $2a_p$, $2a_p$ unit cell (*Cmmm* model of Table 1) was used. At the highest temperature, the tetragonal a_p, a_p, $2a_p$ unit cell ($P4/mmm$ model) was tested improving slightly the quality of the refinement. Other intermediate models that reproduce the superstructure peaks, such as the diagonal perovskite ($\sqrt{2}a_p$, $\sqrt{2}a_p$, $2a_p$) [15,16] were also considered, but they were rejected because of low figures of merit obtained. The observed, calculated, and difference ND profiles at three different temperatures are also shown in Fig. 1. Structural parameters and agreement factors obtained in this analysis are given in Table 2. In all cases, the occupancy of structural sites was consistent with the chemical formula, and the isotropic thermal factors deduced for La, Ti and O were reasonable.

The evolution of the atomic positions with temperature (Fig. 3) showed that the atomic coordinates of the orthorhombic phase approach those of the tetragonal phase as the temperature increases. The Ti coordinates, x/a and z/c, basically did not change, but y/b coordinates of La1 and La2 sites approached 0.25 at the higher temperatures. A similar trend was found for oxygen atoms where z/c coordinates of equatorial O2 and O3 oxygen approached that of O4 oxygen ($z/c = 0.235$), and x/a coordinates of apical oxygen, O1 and O5 came near to $z/c = 0.25$. At 773 K, the atoms had not still reached positions of the tetragonal phase (Table 1). This result suggests that slightly higher temperatures are required to achieve the orthorhombic–tetragonal transformation. In the tetragonal model, only three oxygens, two apicals (OI, OIII) and one equatorial (OII), are distinguished in TiO_6 octahedra (Tables 1 and 2).

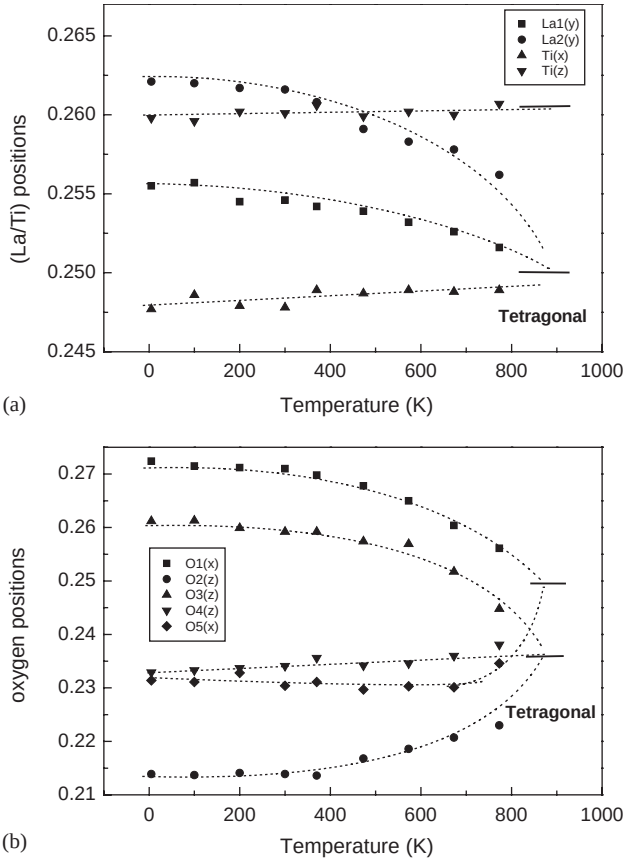

Fig. 3. Temperature dependence of atom positions in the orthorhombic perovskite. La and Ti (a) and of apical and equatorial oxygen (b). Horizontal lines, at the right side, correspond to atom positions deduced with the tetragonal model from the ND pattern recorded at 773 K.

The analysis of Fourier map differences between reflections observed at 5 K and those calculated with the *Cmmm* model, in which Li ions were not included, showed that Li^+ ions are preferentially located at square windows relating contiguous A-sites of the perovskite [17]. In this analysis, it was shown that the probability to occupy square windows at La poor planes is high. However, the probability to occupy those of La rich planes is very low. In this case, the shift of Li ions to square windows located at the plane $z/c = 0.25$ was detected. The analysis of Li location was not possible in perovskites heated above 600 K, because the small amount of Li at structural sites and the high Li mobility.

4. Discussion

The Rietveld analysis of powder ND patterns of $Li_{0.18}La_{0.61}TiO_3$ recorded at increasing temperatures, showed the progressive orthorhombic–tetragonal transformation. In both structures, La and vacancies were ordered in alternating planes along the c-axis, and Ti atoms were shifted from the center of the octahedra

towards the vacancy-rich plane. Both structural features were also deduced from XRD experiments [10,11].

The main difference between low and high temperature structures was the octahedral tilting scheme. Structural views of two phases of $Li_{0.18}La_{0.61}TiO_3$ perovskite, along *a*- and *b*-axes, are given in Fig. 4. Along the *a*-axis there are no big differences between both structures. The main difference is seen along the *b*-axis where oxygen displacements associated with out-of phase tilting of the octahedra are observed.

4.1. Polyhedra distortion

As a consequence of the La distribution in alternating planes, TiO_6 octahedra are clearly distorted and two different Ti–O distances were deduced along the *c*-axis (Ti–O1 $\approx$ 1.87 Å and Ti–O5 $\approx$ 2.02 Å (see Table 2). At increasing temperature the changes produced in TiO_6 octahedra are small: distances corresponding to apical oxygens, Ti–O1 and Ti–O5, increased slightly with temperature and those of equatorial oxygen, Ti–O2, Ti–O3 and Ti–O4 approached a common value at higher temperatures (1.95 Å) (see Table 2). Since octahedral distortion are mainly due to the La distribution in alternated planes and do not change with temperature, differences between two apical Ti–O distances (1.8 and 2.02 Å) remained constant during structural transformation.

In LaO_{12} polyhedra, important modifications were detected between 5 and 773 K. In the orthorhombic phase, cuboctahedra showed five different La–O distances, four with double multiplicity and one with four-fold multiplicity (Fig. 5). According to the preferential location of vacancies in the $z/c = 0.5$ plane, the mean distance calculated for $\langle$ La2–O $\rangle$ = 2.794 Å at 5 K is higher than $\langle$ La1–O $\rangle$ = 2.687 Å. As the temperature increased, the differences of La–O distances decreased. In each cuboctahedra, the two distances of La ions to apical oxygen (O1 or O5) approach to a common value. The same effect is detected for the La–O distances at the equatorial plane (O2, O3 and O4). Consequently, the number of La–O distances were reduced from ten, at

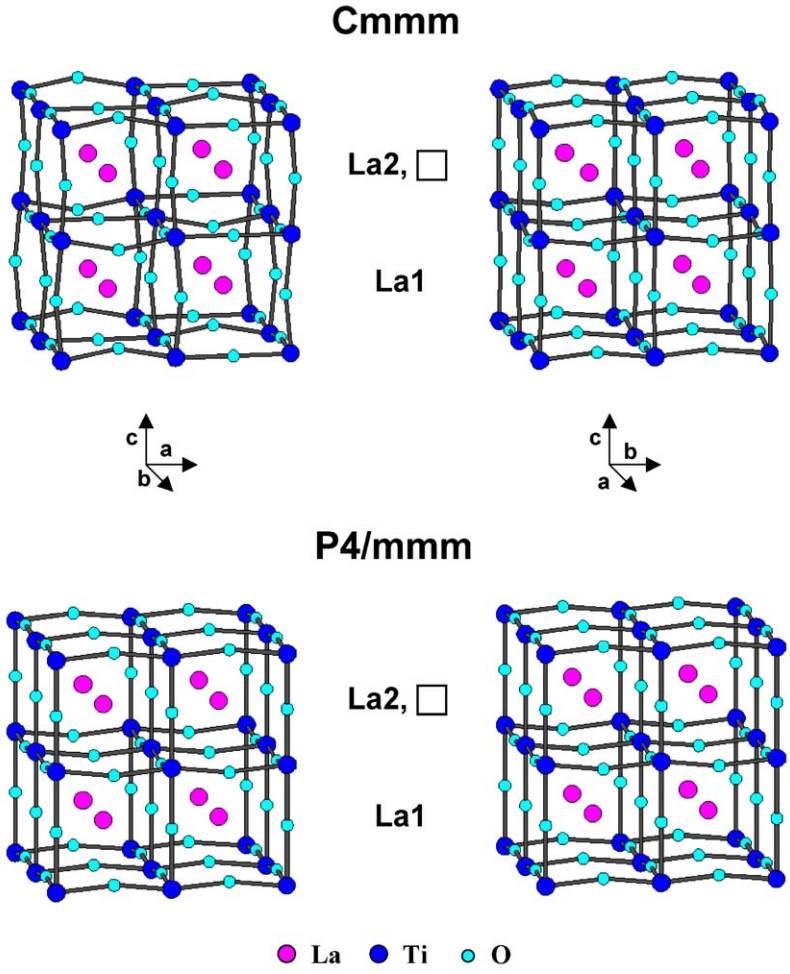

Fig. 4. Crystal structure of $Li_{0.18}La_{0.61}TiO_3$ perovskite along the [010] (left) and [100] directions (right) at 5 K (top) and 773 K (bottom) as deduced from *Cmmm* and *P*4/*mmm* model. The octahedral distortion and the octahedral tilting along the *b*-axis is clearly observed in the low temperature phase. Differences on La coordination in $z/c = 0$ (fully occupied) and 0.5 (partially occupied) planes are illustrated.

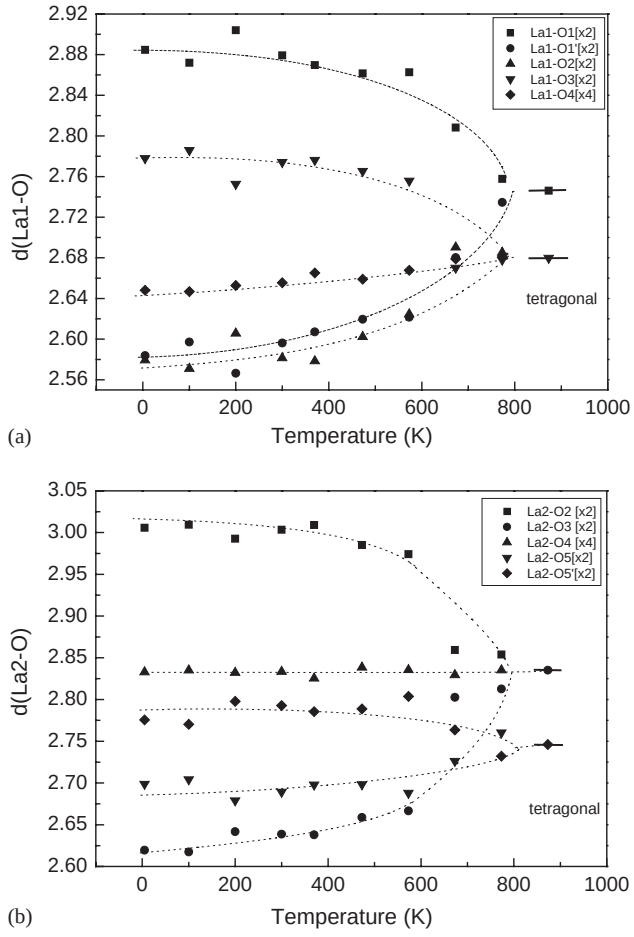

Fig. 5. Evolution of La–O distances with temperature in the orthorhombic perovskite. Distances corresponding to the tetragonal model are indicated by horizontal lines at the right side.

low temperature, to only three at the highest temperature. In the tetragonal model, only two La–O distances are present in each La cuboctahedra. In both LaO_{12} polyhedra, La–O distances are equal in the central plane (La1–OI = La2–OIII = 2.75 Å); but distances of La to O atoms to adjacent planes are notably different (La1–OII = 2.68, La2–OII = 2.84 Å). This difference produces cuboctahedra flattened/elongated in the [001] direction. This distortion is again caused by the ordering of vacancies in alternate planes along the *c*-axis (Fig. 5).

4.2. Octahedral tilting

The main feature of the orthorhombic structure is the out-of phase ($0\varphi0$) tilting of octahedra around the *b*-axis [12,13] ($a^0b^-c^0$ in the Glazer notation [18]). Since Ti cations are shifted from the center of the octahedra, the tilting of octahedra must be estimated from the inclination of O1–O5 direction with respect to the *c*-axis. The study of tilting angles (φ) showed that they decreased in a non-uniform way with temperature (Table 2). This angle remained basically constant, around 5° up to 400 K, and then decreased rapidly above this temperature. However, the presence of residual peaks of the orthorhombic phase in the ND pattern of the sample heated to 773 K, indicated that octahedral tilting has not completely disappeared at this temperature (Table 2).

Similar conclusions were derived by Yashima et al. [19] in the $La_{0.64}(Ti_{0.92}Nb_{0.08})O_3$ perovksite, where octahedral tilting decreased as increasing temperature. In this sample, the high temperature phase was described with the a_p, a_p, $2a_p$ tetragonal unit cell ($P4/mmm$ S.G.). However, in this case the ($2a_p$, $2a_p$, $2a_p$) orthorhombic- (a_p, a_p, $2a_p$) tetragonal transformation was produced at lower temperatures, 650 K, than in our sample.

As a consequence of changes produced in the octahedral tilting, the thermal expansion of the unit cell became anisotropic. Below 400 K, the three crystallographic axes showed a similar thermal expansion, whereas above this temperature, the expansion of the *b*-axis was clearly lower than those of the *a*- and *c*-axes. Given that the octahedral tilting takes place around the *b*-axis, the modification of the octahedral tilting only affect to *a*- and *c*-axes.

Changes in the octahedral tilting produced important modifications of the geometry of the square windows that connect contiguous *A* sites of the perovskite. It is interesting to correlate structural modifications to Li conductivity reported previously [3,5]. In the orthorhombic phase, the octahedral tilting produced four different square windows along the *b*-axis, two along *a*-axis and only one along the *c*-axis (Fig. 6). Table 3 includes diagonal O–O distances of square windows at 5 K. As a consequence of the low occupancy of La2 sites, diagonal O–O distances of square windows that connect contiguous *A*-site at $z/c = 0.5$ plane are greater than those at the $z/c = 0$ planes. From this fact, Li mobility should be enhanced in planes $z/c = 0.5$.

The differences between two diagonal distances produces a rhombic deformation of square windows. From the analysis of different square windows of the low temperature phase, it was concluded that Li mobility must be favored along the *a*-axis in $z/c = 0.5$ planes, where square windows are less distorted (3.88–4.15 Å) than those along the *b*-axis (3.58–4.45 and 3.71–4.13 Å). In the [010] direction, the alternating rotation of contiguous octahedra reduces also the cross section for Li diffusion (see Fig. 6). In the *c*-axis, diagonal distortion of square windows is smaller (3.82–3.95 Å); but the presence of alternating La-rich planes hinders Li diffusion along this axis.

As temperature raised, the octahedral tilting decreases and the 12 different diagonal O–O distances along the *b*- and *a*-axes converge into three (Fig. 7), reducing the number of square windows from six to three in the tetragonal phase. In this phase, diagonal O–O distances

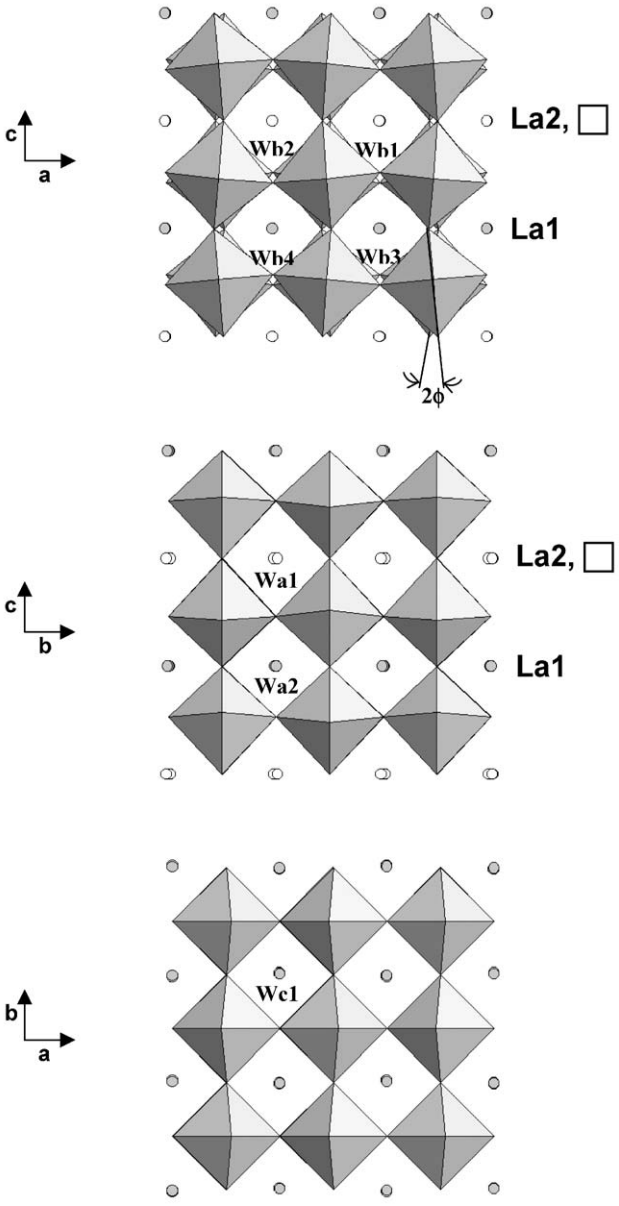

Fig. 6. Structural views along the three crystallographic axes of the $Li_{0.18}La_{0.61}TiO_3$ perovskite as deduced from neutron diffraction data obtained at 5 K. The octahedral tilting produced along the *b*-axis is also indicated.

of square windows at $z/c = 0$, labeled as Wb_1, Wb_2 and Wa_1, become similar at high temperature (see Figs. 3 and 6). A similar trend is observed in square windows of the $z/c = 0.5$ plane, labeled as Wb_3, Wb_4 and Wa_2. As a consequence of the different size of square windows at $z/c = 0$ and 0.5 planes (3.694×3.884 and 3.884×4.132 Å), the two-dimensional motion of Li in alternating planes is preserved in the tetragonal phase.

At 5 K, Li ions are located at square windows (bottlenecks) that connect contiguous *A*-sites of the perovskite. However, at increasing temperatures, oxygen local motions increase destabilizing Li coordination at square windows; from this fact lithium conductivity is considerably improved. At this point, it is interesting to analyze the variation of isotropic thermal factors of atoms (B_{iso}) with temperature (Fig. 8). At every measured temperature the thermal oxygen factors are higher than those of the La and Ti ions. Thermal factors of La ions increased in a linear way; however, thermal factors of O and Ti atoms increase more rapidly above 400 K. These results suggest that high dc-conductivity values reported at this temperature in this sample is a consequence of the local motions of octahedra than destabilize the Li coordination at square windows of the perovskite.

Table 3
Diagonal O–O distances of square windows that connect contiguous *A*-sites along three axes deduced with orthorhombic and tetragonal models

Phase	Direction	z/c	Window label	Oxygen diagonal windows	d_{O-O} (Å)
Orthorhombic	[001]	—	Wc_1	O4–O4	3.859
		—		O3–O2	3.888
	[100]	0.5	Wa_1	O4–O4	4.145
				O5–O5	3.880
		0	Wa_2	O4–O4	3.626
				O1–O1	3.885
	[010]	0.5	Wb_2	O2–O2	4.453
				O5–O5	3.578
			Wb_1	O3–O3	3.710
				O5–O5	4.140
		0	Wb_4	O2–O2	3.320
				O1–O1	4.206
			Wb_3	O3–O3	4.061
				O1–O1	3.512
Tetragonal	[001]	—	Wc_1	OII–OII	3.884
		—		OII–OII	3.884
	[100]/[010]	0.5	Wa_1	OII–OII	3.884
				OIII–OIII	4.132
		0	Wa_2	OII–OII	3.694
				OI–OI	3.884

In both phases, information about planes $z/c = 0$ and 0.5 is differentiated.

5. Concluding remarks

The analysis of ND patterns recorded at increasing temperature in the Li-poor $Li_{0.18}La_{0.61}TiO_3$ perovskite, showed that the $2a_p$, $2a_p$, $2a_p$ orthorhombic structure tends towards that of the a_p, a_p, $2a_p$ tetragonal phase. In this transformation, the octahedral tilting around the *b*-axis progressively disappears, and La ions shifted to special ((0,0,0) and (0,0,1/2)) positions of the tetragonal phase. However, in this phase, the arrangement of La and vacancies in alternating planes along the *c*-axis was not affected.

The octahedral tilting in the orthorhombic phase, ($a^o b^- c^o$ in the Glazer notation) produced different

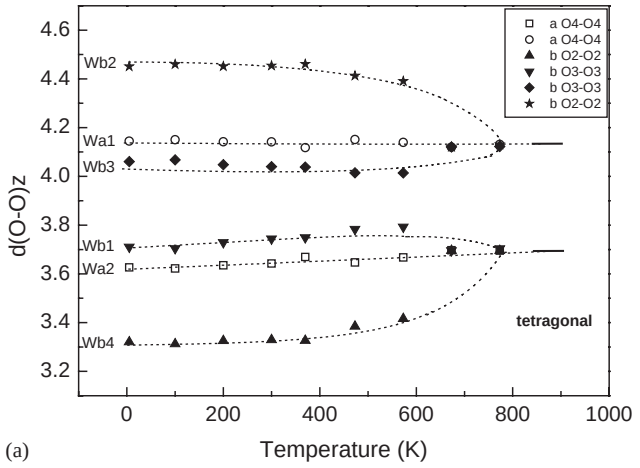

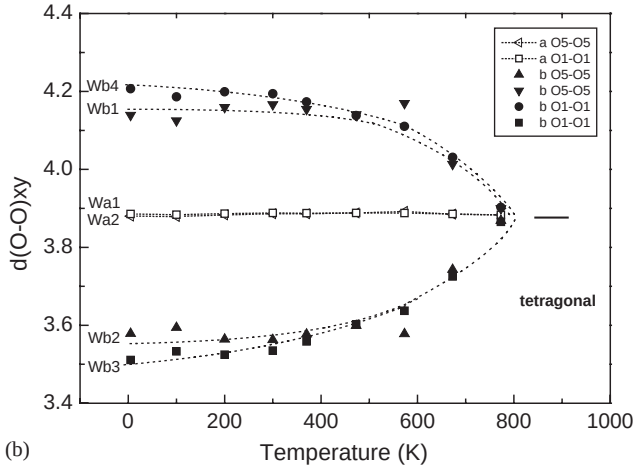

Fig. 7. Temperature dependence of O–O diagonal distances in square windows that connect contiguous *A*-sites along the [001] (a) and along [010] and [100] directions (b). Dotted lines are given as eye-guidelines. Distances corresponding to the tetragonal model are indicated by horizontal lines.

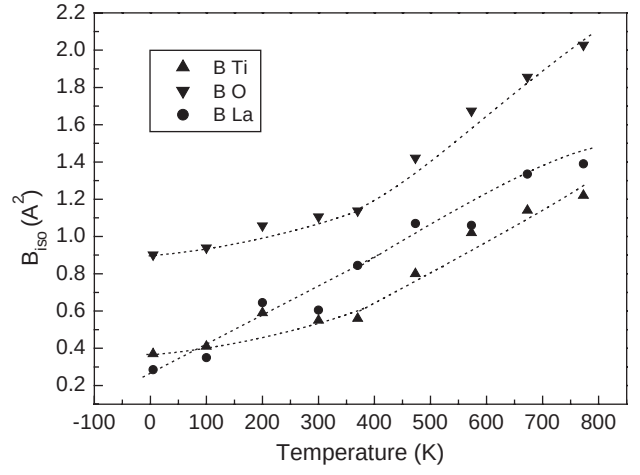

Fig. 8. Averaged isotropic thermal factors of La, Ti, and O ions in the orthorhombic phase as a function of temperature.

square windows along the three crystallographic axes. As a consequence of the window distortion, the mobility along the *a*-axis must be favored in this phase. The number of square windows is reduced to three as temperature increases, favoring a two-dimensional motion of lithium at 773 K in alternating planes of the perovskite. The two-dimensional mobility of Li-poor members contrasts with the three-dimensional one of the Li-rich samples, where the distribution of La-vacancies is disordered.

Acknowledgments

The authors thank M.L. Sanjuán for helpful discussions and ILL for the provision of neutron beam time. We thank the Spanish Agency CICYT (MAT2001-3713-C04-03 project) for the financial support.

References

[1] A.G. Belous, G.N. Novitskaya, S.V. Polyanetskaya, Y.I. Gornikov, Zh. Neorg. Khimii 32 (1987) 283.
[2] Y. Inaguma, L. Chen, M. Itoh, T. Nakamura, T. Uchida, H. Ikuta, M. Wakihara, Solid State Commun. 86 (1993) 689–693.
[3] M.A. Paris, J. Sanz, C. Leon, J. Santamaría, J. Ibarra, A. Varez, Chem. Mater. 12 (2000) 1694–1701.
[4] A.I. Ruiz, M.L. López, M.L. Veiga, C. Pico, Solid State Ionics 112 (1998) 291–297.
[5] A. Rivera, C. León, J. Santamaría, A. Varez, M.A. Paris, J. Sanz, J. Non-Cryst. Solids 992 (2002) 307–310.
[6] M. Itoh, Y. Inaguma, W.H. Jung, L. Chen, T. Nakamura, Solid State Ionics 70–71 (1994) 203–207.
[7] H. Kawai, J. Kuwano, J. Electrochem. Soc. 141 (1994) L78–L79.
[8] A.D. Robertson, S. García-Martín, A. Coats, A.R. West, J. Mater. Chem. 5 (1995) 1405–1412.
[9] Y. Harada, Y. Hirakoso, H. Kawai, J. Kuwano, Solid State Ionics 121 (1999) 245–251.
[10] J.L. Fourquet, H. Duroy, M.P. Crosnier-López, J. Solid State Chem. 127 (1996) 283–294.
[11] J. Ibarra, A. Várez, C. León, J. Santamaría, L.M. Torres-Martinez, J. Sanz, Solid State Ionics 134 (2000) 219–228.
[12] Y. Inaguma, T. Katsumata, M. Itoh, Y. Morii, J. Solid State Chem. 166 (2002) 67–72.
[13] J. Sanz, J.A. Alonso, A. Várez, M.T. Fernández-Díaz, Dalton Transact. (2002) 1406–1408.
[14] A. Várez, J. Ibarra, A. Rivera, C. León, J. Santamaría, M.A. Laguna, M.L. Sanjuán, J. Sanz. Chem. Mater. 15 (2003) 225–232.
[15] A. Várez, F. García-Alvarado, E. Morán, M.A. Alario-Franco, J. Solid State Chem. 118 (1995) 78–83.
[16] J.M.S. Skakle, G.C. Mather, M. Morales, R.I. Smith, A.R. West, J. Mater. Chem. 5 (1995) 1807–1808.
[17] A. Várez, Y. Inaguma, M.T. Fernández-Díaz, J.A. Alonso, J. Sanz. Chem. Mater. 15 (2003) 4637–4641.
[18] A.M. Glazer, Acta Crystallogr. B 28 (1972) 3384–3392.
[19] M. Yashima, M. Mori, T. Kamiyama, K.-I. Oikawa, A. Hoshikawa, S. Torii, K. Saitoh, K. Tsuda, Chem. Phys. Lett. 375 (2003) 240–246.